Uniform flow injection into a turbulent boundary layer for trailing edge noise reduction

Máté Szőke,[1, a)] Daniele Fiscaletti,[1] and Mahdi Azarpeyvand[1]

University of Bristol, Bristol, United Kingdom, BS8 1TR

(Dated: 22 July 2020)

The hydrodynamic effects of inclined uniform continuous blowing on a turbulent boundary layer are investigated experimentally. A laminar flow is introduced into the boundary layer through a fence on a flat plate at a distance of $3.38\delta_0$ upstream of the trailing edge. The effects of this open-loop technique of flow control are examined at different angles of injection and at different blowing rates. Surface pressure fluctuations acquired from flush-mounted microphones are used to estimate the trailing edge noise. Injection angles of 70° and 90° in combination with strong blowing rates enable a noise reduction of up to 15 dB at mid and high frequencies, $f > 300$ Hz. Similar aeroacoustic performances are obtained at a blowing angle of 50°, but at lower blowing rates. At low frequencies a penalty is expected, with the trailing edge noise increasing for all the injection angles and blowing rates under analysis. Mean velocity profiles from hot-wire anemometry reveal that high injection angles and strong blowing rates induce a flow separation which is expected to deteriorate the aerodynamic performances. When applying a uniform blowing at 50°, however, no flow separation occurs. From an aeroacoustic and aerodynamic point of view, uniform blowing applied at 50° and at intermediate blowing rates is found to be the most promising setting.

[a)]Electronic mail: m.szoke@vt.edu; currently at Aerospace and Ocean Engineering, Virginia Tech, Blacksburg, VA, 24061, USA.

I. INTRODUCTION

Sound generated by turbulence around an airfoil represents one of the dominant sources of noise from airplanes, turbomachines, and wind farms[1–4]. Brooks *et al.*[2] identified the turbulent boundary layer trailing edge (TE) noise as one of the dominating component of airfoil self noise. With the aim of mitigating the trailing edge noise, several studies were conducted since the 1970s[1,5–9]. These pioneering works revealed the mechanism of trailing edge noise generation. It was shown that as the hydrodynamic pressure field associated with the turbulent boundary layer passes over the sharp trailing edge, the pressure field scatters into sound in a dipolar manner. In relation to this mechanism, a technique of noise reduction could act either on (i) the scattering conditions, or on (ii) the pressure field within the boundary layer upstream of the trailing edge. This observation led to the development of various TE noise reduction methods, which can be classified under two main categories, depending on the strategy that they rely on: (i) *passive methods*, where the physical and geometrical properties of the trailing edge are altered, such that the efficiency of the noise scattering is reduced, and (ii) *active methods*, which target the alteration of the hydrodynamic pressure field within the turbulent boundary layer upstream of the trailing edge. Examples of passive methods are the trailing edge serrations[10–16], trailing edge brushes[17,18], porous materials[19–27], surface treatments[28–33], shape optimization, morphing[34,35], etc. Passive methods are often tailored to a given range of conditions (Reynolds number, angle of attack, etc.), and outside of this range they might experience a reduction of their aeroacoustic performances. Additionally, should the noise reduction requirements change during machine operation, passive methods cannot be adjusted. Active methods, on the other hand, can allow adjustment according to the device operational condition and the required noise reduction. Their other advantage is that they may also be used for the purpose of improving the aerodynamic performance. However, their main drawback is that they require a supply of external energy[36,37]. While passive noise reduction methods have received a significant attention from the research community, active methods are in their early stages of development. Most commonly, previous works focused on the use of flow suction from[4,38–40], or flow injection into the boundary layer[41,42]. The main drawback of flow suction is that it requires a significant amount of air to be removed from the boundary layer, namely, it was found that removing approximately 60% of the boundary layer thickness provides the best aeroacoustic performance[40,43]. A potential solution to overcome this issue is to employ flow injection into the boundary layer upstream of the trailing edge. However, the number of studies investigating the

use of blowing with the aim of reducing the TE noise is scarce to date[41,42]. These works have shown that the use of blowing can result in trailing edge noise reduction, but the underlying noise reduction mechanism which flow injection relies on is yet to be understood.

Studying the effects of flow injection on the turbulence within a boundary layer is the first step toward interpreting how flow injection can reduce the trailing edge noise. Flow injection into a turbulent boundary layer has previously been studied in the literature[44–49], but only a limited number of studies focus on uniform injection into high Reynolds number (on the order of millions) turbulent boundary layers, which are of main interest to applications where TE noise is relevant. Among the limited number of works examining how turbulence changes as a result of flow injection, two works offer a rather detailed discussion on this problem. Namely, the numerical studies presented by Park and Choi[44] and by Kametani and Fukagata[45] shed light on the effects of perpendicular flow injection on boundary layer turbulence. Both studies investigated the changes in various turbulence quantities, such as turbulence budget, skin friction, turbulence intensity, boundary layer thickness, Reynolds shear stresses, convection velocity, only to mention a few. These numerical works revealed that blowing reduces the skin friction in the vicinity of the blowing slit, and it lifts the streamwise vortices away from the wall. As the vortices move away from the wall, they experience a drop in the viscous diffusion. As a result, turbulence intensity increases together with the skin friction downstream of the flow control area. Lifting the turbulent motions away from the wall may potentially reduce trailing edge noise, because boundary layer turbulence is the fundamental source of trailing edge noise generation[32,38,42]. These early studies, however, lack detailed hydrodynamic pressure field analysis and are also limited to perpendicular flow injection.

In this work, we seek an explanation to the underlying noise reduction mechanism of inclined blowing. To do so, we investigate experimentally the hydrodynamic effects of uniform inclined flow injection into a turbulent boundary layer over a zero pressure gradient flat plate of finite length. We apply flow injection at various injection angles, which is defined with respect to the free-stream velocity, and we independently vary the rate of flow injection at all injection angles. Hot-wire anemometry and flush-mounted microphones are used to measure the velocity and surface pressure fluctuations associated with the boundary layer. The effects of inclined uniform blowing on the trailing edge noise generation are evaluated using Amiet's far field trailing edge noise model[9].

The current paper is organised as follows. Section II describes the measurement conditions,

the experimental set-up, the geometrical properties relevant to the experimental investigation, and illustrates Amiet's model, which is used in this work to estimate the far field trailing edge noise. In Section III, we present the predicted far field noise for different conditions of flow injection. Section IV provides an explanation for why and how changing the injection parameters affects the trailing edge noise. To address these aspects, the flow structure developing downstream of the flow control section is investigated.

II. EXPERIMENTAL APPROACH

Experiments were conducted on a zero-pressure-gradient flat plate test rig in the open-jet wind tunnel of the University of Bristol. The closed-loop wind tunnel has a circular nozzle with a diameter of 1.1 m, and a 2 m long test section, and it is capable of producing flow speeds up to 26 m/s with an incoming flow turbulence intensity below 0.5%. The flat plate test rig has a length of $L = 1$ m and a width of $W = 0.7$ m, and it ends in a sharp (12°) TE, see Fig. 1. An 80-grit sandpaper was placed immediately after the plate semi-elliptical leading-edge to trigger the development of the turbulent boundary layer on the surface of the plate. Downstream the flow tripping, the boundary layer passes over the blowing area, where flow blowing is applied in an open-loop manner. The rig is instrumented with flush-mounted microphones downstream of the flow suction area. Tests were carried out at the uniform flow velocity of $u_\infty = 15$ m/s, corresponding to a Reynolds number of approximately $Re_L = 10^6$ based on the length of the plate ($Re_L = u_\infty L/\nu$). In this work, this flow velocity was chosen because it gave the highest signal to noise ratio between the surface pressure fluctuations and the background noise.

A. Test rig and instrumentation

In Figure 1, a geometrical description of the rig and the coordinate system can be observed. A coordinate system is introduced, which consists of the streamwise (x), the wall-normal (y), and the spanwise (z) directions, with its origin located at the mid-span of the plate, at the downstream edge of the active flow control section. The surface pressure fluctuations and the streamwise component of the velocity were measured simultaneously in the vicinity of the flat plate trailing edge. A total number of 7 pressure transducers (Knowles FG-23329-P07 type microphones) were embedded into the surface of the rig to capture the surface pressure fluctuations. Four microphones were

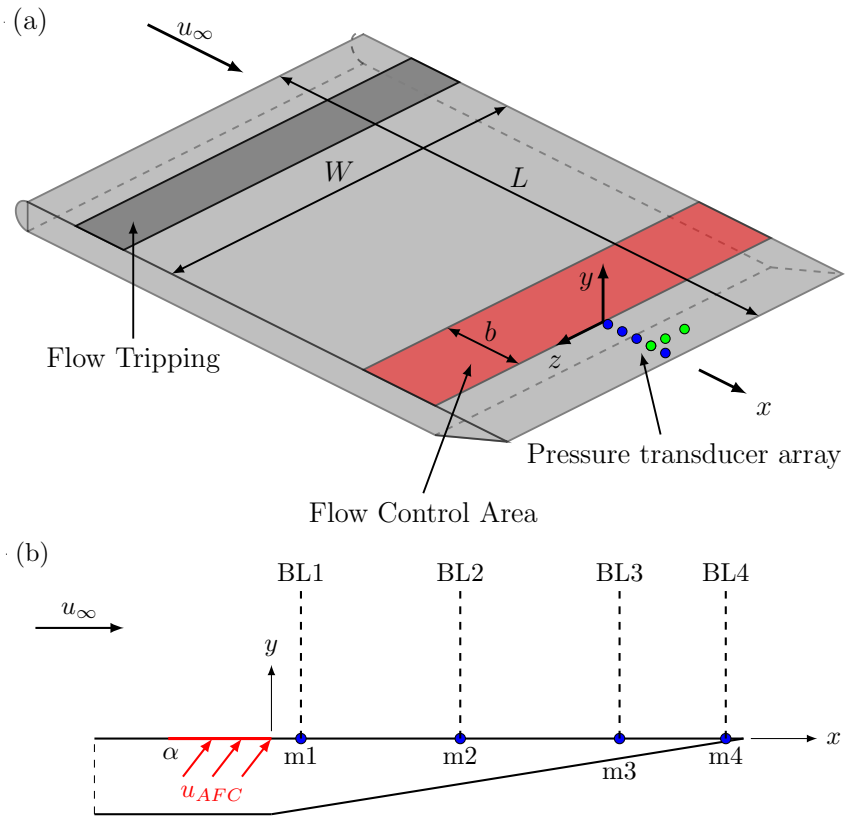

FIG. 1. (a) The schematics of the rig, and (b) the area downstream of the flow control section where the simultaneous velocity and pressure measurements were performed at locations BL1-BL4.

positioned along the streamwise, and three along the spanwise direction in the vicinity of the TE, as schematically shown in Fig. 1. The streamwise component of the velocity was measured using hot-wire anemometry with the aim of characterising the boundary layer flow downstream of the flow control area. Single-sensor hot-wire probes of type Dantec 55P16 were operated by a Dantec StreamWare Pro CTA91C10 module. The hot-wire probe was positioned above four different flush-mounted microphones as illustrated in Fig. 1(b), and the hot-wire sensor was traversed along the wall-normal direction (y) using a ThorLabs LTS300/M stage, with a positioning accuracy of 5 μm. Data from the sensors (microphones and hot-wire probe) were acquired using a National Instruments PXIe-4499 system at a sampling rate of $65,536$ ($=2^{16}$) samples/sec for a time span of 16 sec at each measurement point. Data processing was performed with the use of Python's SciPy package.

The flow behavior in the vicinity of the trailing edge was studied prior to investigating the effects of flow injection on boundary layer turbulence. Our thorough flow assessment analysis,

consisting of hot-wire anemometry, static pressure (not presented here for brevity), and unsteady surface pressure measurements, found pieces of evidence that a zero pressure gradient turbulent boundary layer develops over the surface of the flat plate test rig. These observations confirmed that the flat plate test rig is a suitable tool to study the aeroacoustic effects of flow injection. For a more detailed description of the baseline case, test rig and measurement apparatus, we refer to Refs.[40,42,50,51].

B. Uniform blowing parameters

Inclined uniform blowing is applied upstream of the sharp TE to manipulate the turbulent boundary layer flow. In order to have an inclined injection of air, a honeycomb structure is installed within the surface of the plate. The size of the pores within the honeycomb structure is 5 mm $\times$ 5 mm, the thickness of the walls between the neighbouring cells is 0.5 mm, and the overall depth of the honeycomb structure is 10 mm. Inclining the pores of the honeycomb structure ensures an inclined direction of flow with respect to the free-stream flow. Specifically, the honeycomb pores are oriented in the downstream direction. Four different blowing angles (α) are considered in this experimental work, namely, $\alpha = 30^\circ, 50^\circ, 70^\circ$, and 90°. The section of air injection was covered by a wire mesh to ensure that the surface of the flow control section remains smooth. The wire mesh was made of square weaved stainless steel with a filament diameter of 0.1 mm and pore size of 0.2 mm. Preliminary tests showed that the described configuration of the flow control unit did not introduce any additional perturbation to the boundary layer. In particular, the presence of the flow control section (honeycomb and wire mesh) caused no quantifiable change to the surface pressure fluctuations when compared to the case where the flow control section was replaced using a smooth plate.

The velocity of the flow injection (u_{AFC}) was measured using hot-wire anemometry with the sensor positioned at a distance of approximately 1 mm above the surface of the flow control area while the wind tunnel fan was turned off. A radial fan, whose power was computer-controlled, enabled the fine adjustment of the blowing velocity. From this, the injection velocity (u_{AFC}) was obtained and used to determine the flow control severity, σ. The nature of the wind tunnel used in this study implies that the absolute static pressure in the test volume is nearly identical to the ambient pressure, therefore, the presence of the flow is concluded to have a negligible effect on the flow injection velocity.

	BL1	BL2	BL3	BL4	TE
x/δ_0 (-)	0.29	1.48	2.66	3.25	3.38

TABLE I. Streamwise locations of the simultaneous velocity and surface pressure measurement.

The flow control severity relates the momentum deficit of the boundary layer to the momentum of the flow control system. According to Antonia *et al.*[52], the *flow control severity* is defined as follows:

$$\sigma = \frac{u_{AFC} b}{u_\infty \theta_0}, \tag{1}$$

where u_{AFC} is the magnitude of the mean flow control velocity, $b = 30$ mm is length of the flow control section along the streamwise direction, u_∞ is the velocity of the free-stream flow, and $\theta_0 = 2.6$ mm is the momentum thickness of the non-disturbed boundary layer at location BL1.

In this study, two different sets of measurements were performed. In the first set of measurements, signals from all flush-mounted microphones were simultaneously recorded for a range of flow injection velocities ($u_{AFC} = 0.1u_\infty$ to $0.3u_\infty$) and inclination angles ($\alpha = 30^\circ, 50^\circ, 70^\circ$ and 90°). The measurement of the surface pressure fluctuations is in support of estimating the generated levels of trailing edge noise, as will be discussed in Section II C. During the second set of measurements, the streamwise velocity was measured with hot-wire anemometry along the whole wall-normal span of the turbulent boundary layer thickness (δ), at four different streamwise locations (x/δ_0), marked as BL1, BL2, BL3 and BL4, see the dashed lines in Fig. 1(b). At BL1 through BL4, the streamwise velocity and surface pressure fluctuations were recorded simultaneously to develop a comparative analysis of the turbulence characteristics and of the hydrodynamic pressure field. The thickness of the undisturbed boundary layer (δ_0) was measured at location BL1 without flow injection ($u_{AFC} = 0$ m/s). This reference parameter is defined as $u(y = \delta_0) = 0.98u_\infty$, and the resulting boundary layer thickness was found to be $\delta_0 = 34$ mm. The streamwise locations of BL1-BL4 and the trailing edge (TE) are given in Table I.

C. Amiet's trailing edge noise model

The direct measurement of the far field TE noise requires the use of an anechoic wind tunnel. Nonetheless, several physical models were developed in the last few decades[2,9,53], which enable us to estimate the far field noise from the flow characteristics. According to these models, pressure

and velocity measurements from conventional wind tunnel tests can be used as input parameters to confidently estimate the far field TE noise. In this work, we will make use of the Amiet's TE noise model[9].

Amiet's model states that the spectral content of the trailing edge noise (S_{pp}) at a far field distance from the TE center-line of the flat plate ($x, y, z = 0$) can be estimated using the following equation:

$$S_{pp}(x, y, z = 0, f) = \left(\frac{fLy}{4\pi c_0 \xi^2}\right)^2 \frac{W}{2} |\mathscr{L}|^2 \Lambda_z(f) \phi_{pp}(f), \tag{2}$$

where f denotes the frequency, c_0 is the speed of sound, $\xi^2 = x^2 + (1 - u_\infty/c_0)^2 y^2$ is the convection-corrected far field observer position, L is the length of the plate (chord), W is the width of the plate, $\mathscr{L}$ is the gust response transfer function[54], Λ_z and ϕ_{pp} are, respectively, the spanwise extent of the turbulent structures within the boundary layer, and the power spectrum of the surface pressure fluctuations near the TE. Amiet's model works under the assumption of stationary turbulence. A more detailed description and the derivation of the model is given by Amiet[7,9]. From Amiet's model, the product $\Lambda_z \phi_{pp}$ drives the generated far field noise. Therefore, the reduction of this product is the ultimate goal of any TE noise reduction technique.

In the present work, the power spectrum of the surface pressure fluctuations (ϕ_{pp}) was directly measured, while the spanwise extent of the turbulent structures (Λ_z) could be calculated from the pressure signals as follows[9]:

$$\Lambda_z(f) = \int_0^\infty \sqrt{\gamma_z^2(f, \zeta)} \mathrm{d}\zeta, \tag{3}$$

where $\gamma_z^2(f, \zeta)$ represents the spanwise coherence of surface pressure fluctuations acquired from two microphones located in the proximity to the TE, with a spanwise separation distance of $\zeta = \Delta z$. The coherence (normalized cross-spectrum) could be interpreted as the spanwise extent of turbulent structures. In the current work, the spanwise coherence was measured at a streamwise distance of $0.4\delta_0$ upstream the TE. At this streamwise location, the thickness of the trailing edge is sufficiently large to fully embed the microphones into the rig, therefore they do not introduce any disturbances to the flow traveling below the plate. To calculate the spanwise coherence at different Δz, microphone signals acquired at three spanwise spacings were considered, namely at $\Delta z/\delta_0 = 0.12, 0.26$ and 0.38. From this, the estimation of Λ_z was possible using Eq. (3) and a trapezoidal integration scheme.

III. THE FAR FIELD TRAILING EDGE NOISE

The effects of inclined flow injection on trailing edge noise from the zero-pressure-gradient flat plate is evaluated using Amiet's model[9]. According to the model, the product between the surface pressure spectra (ϕ_{pp}) and the spanwise extent of the turbulent length scales (Λ_z) governs the generation of the far field trailing edge noise. In the following, we analyze and discuss the effects of uniform blowing on each of these quantities and on the estimated TE noise.

A. The power spectra of the surface pressure fluctuations

In order to better understand the effects of flow blowing on the noise generation mechanism, the unsteady surface pressure fluctuations at different streamwise locations downstream of the flow injection area are studied first. The surface pressure spectra for flow injection angles of (a) $\alpha = 90^\circ$, (b) $\alpha = 70^\circ$, (c) $\alpha = 50^\circ$ and (d) $\alpha = 30^\circ$ and at locations BL1 to BL4 are presented in Fig. 2. As can be observed, uniform blowing reduces the energy content of the surface pressure fluctuations at the mid to high frequencies (f >400 Hz). However, the pressure fluctuations show a general increase of energy content at low frequencies (f <400 Hz). This general behaviour is observed at each of the examined injection angles, although the crossing frequency ($f \approx 400$ Hz) and the amount of energy reduction or energy increase are sensitive to both the injection angle (α) and flow control severity (σ). In particular, it appears that uniform blowing at $\alpha = 30^\circ$ produces only a modest attenuation, which also begins to occur at a higher crossing frequency as compared to other angles. The spectra of the surface pressure fluctuations at blowing angles of $\alpha = 90^\circ$ and at $\alpha = 70^\circ$ are quite similar. In addition, when observing locations BL2 through BL4, the shape and the magnitudes of the spectra are found to be similar. This observation suggests that blowing has a long-lasting effect on the flow downstream of the flow control area. The most significant differences exist for a $\alpha = 90^\circ$ blowing angle.

B. The spatial extent of the turbulent structures

An estimation of the spanwise extent of the turbulent structures within the boundary layer (Λ_z) can be obtained using Eq. (3). It can be observed in Fig. 3 that blowing affects the spanwise extent of the boundary layer turbulent structures in a broadband manner. In the case of $\alpha = 90^\circ$, the effect of blowing on Λ_z is modest for $\sigma = 0.9$ and for $\sigma = 1.5$. As the blowing rate increases, a transition

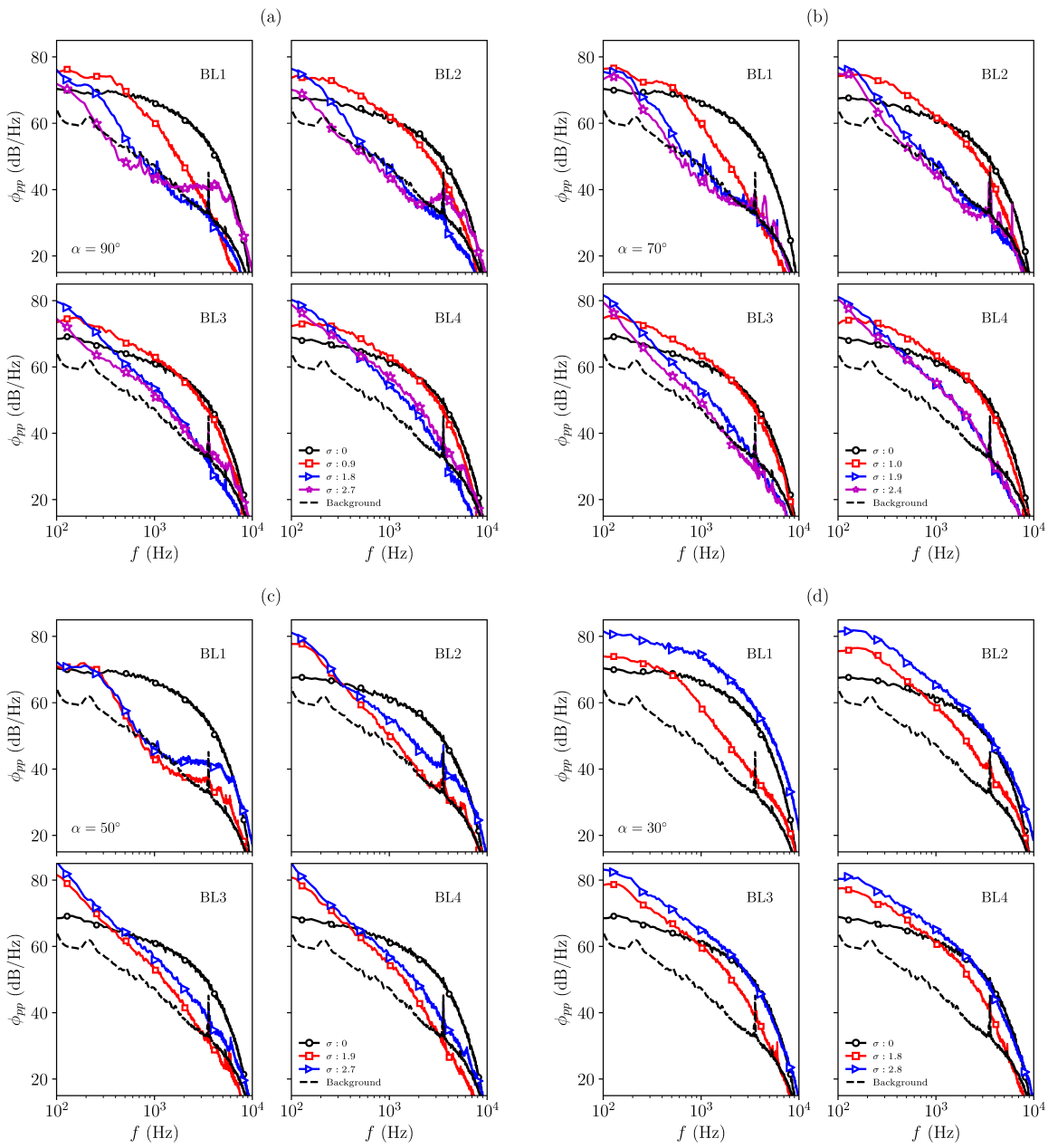

FIG. 2. Surface pressure power spectral density for flow injection angles of (a) $\alpha = 90°$, (b) $\alpha = 70°$, (c) $\alpha = 50°$ and (d) $\alpha = 30°$ at locations BL1-BL4.

occurs in the behavior of the Λ_z curves, see $\sigma = 1.8$. In particular, Λ_z shows an increase at low frequencies ($f < 300$ Hz) and a reduction at high frequencies. Further increasing σ then leads to an emergence of a broadband drop in Λ_z, see for example $\sigma = 2.5$, $\sigma = 2.7$ and $\sigma = 3.2$ in Fig. 3(a). This sudden drop in Λ_z suggests a significant change in the boundary layer flow structure. This assumption is further investigated in Section IV. The same trend as for $\alpha = 90°$ can be observed

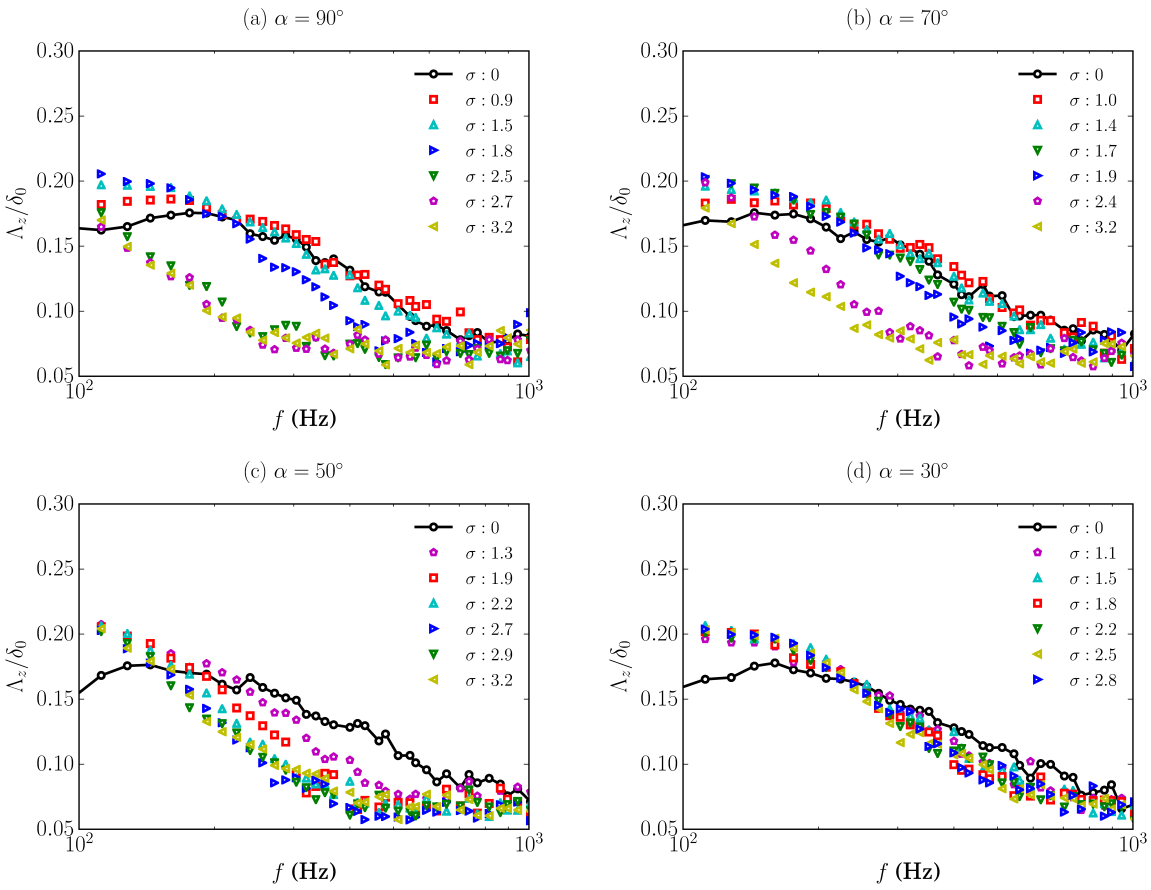

FIG. 3. Estimation of spanwise extent of the turbulent structures (Λ_z) at BL4, i.e. at $x/\delta_0 = 2.98$ with the TE at $x/\delta_0 = 3.38$, for flow injection angles of (a) $\alpha = 90°$, (b) $\alpha = 70°$, (c) $\alpha = 50°$ and (d) $\alpha = 30°$.

at $\alpha = 70°$, see Fig. 3(b). The effect of the blowing rate on Λ_z, however, is mild at $\alpha = 50°$, see Fig. 3(c). At $\alpha = 50°$, applying a uniform blowing leads to a larger Λ_z at low frequencies and to a smaller Λ_z at high frequencies, with $f \approx 250$ Hz being the crossing frequency. This is independent of the blowing rate. Therefore, unlike at $\alpha = 90°$ and $70°$, a sudden drop of Λ_z at high blowing rates is not observed. At a blowing angle of $\alpha = 30°$, the curves are almost identical to each other when considering different blowing rates. This suggests that the developing flow structure in the case of $\alpha = 30°$ is independent of σ. Overall, analogies can be found between injection angles $\alpha = 90°$ and $\alpha = 70°$ on one side, and between injection angles $\alpha = 50°$ and $\alpha = 30°$ on the other side.

C. The estimated far field noise

The far field noise (S_{pp}) is estimated for an observer located at 1 m above the trailing edge using Amiet's model[9]. Far field noise results are presented at different blowing rates and injection angles in Figure 4. As was shown by Amiet[9], the generation of the trailing edge noise is driven by the product of the boundary layer quantities ϕ_{pp} and Λ_z, and therefore a reduction of the product of these two terms can result in the attenuation of the far field trailing edge noise. In general, Fig. 4 exhibits a trend analogous to the surface pressure spectra presented previously, see Fig. 2. This suggests that the term ϕ_{pp} plays a dominant role in the trailing edge noise.

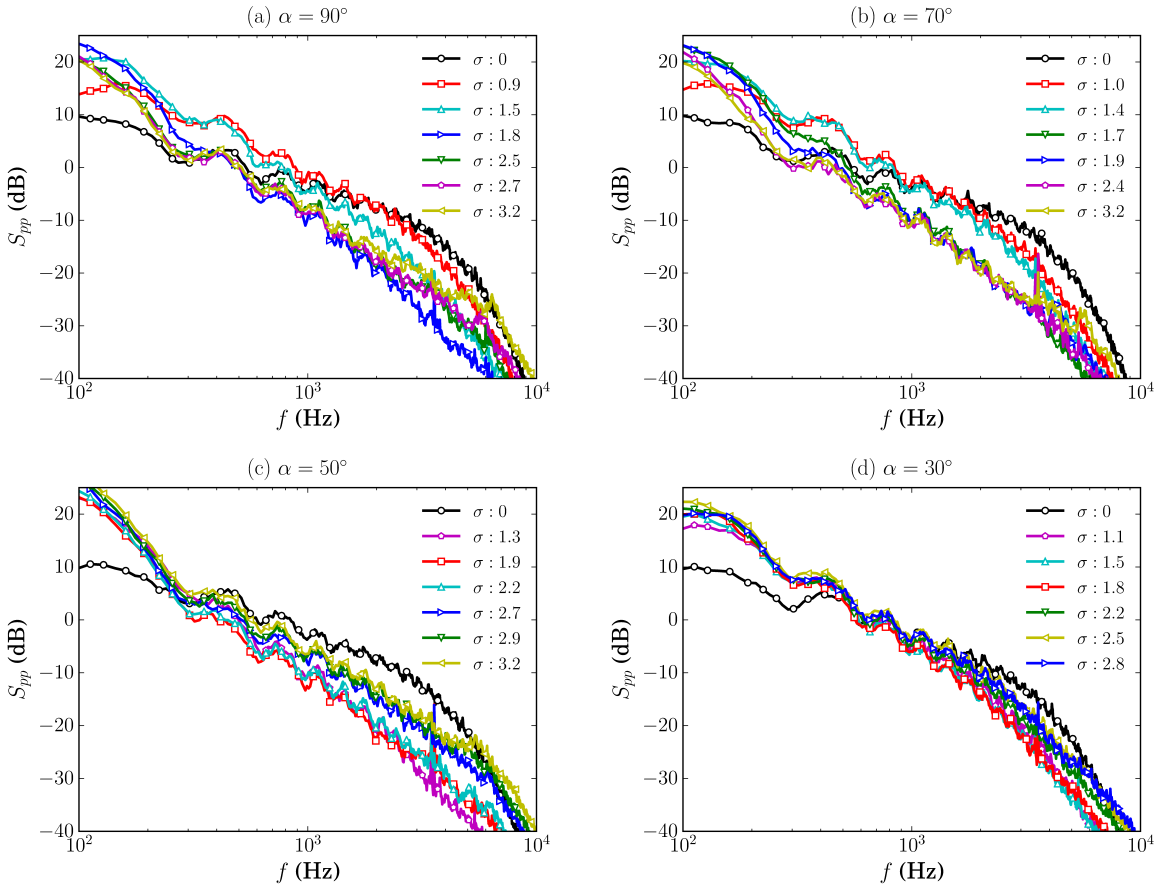

FIG. 4. Estimation of far field noise (S_{pp}) for flow injection angles of (a) $\alpha = 90°$, (b) $\alpha = 70°$, (c) $\alpha = 50°$ and (d) $\alpha = 30°$ using Amiet's trailing edge noise model with the observer located at a vertical distance of 1 m above the trailing edge.

In the case of the perpendicular blowing, i.e. $\alpha = 90°$, low blowing rates ($\sigma = 0.9$ and $\sigma = 1.5$) produce an increase of the far field noise at low frequencies $f < 1$ kHz, and a moderate reduction

at higher frequencies, see Fig. 4(a). As the blowing rate increases to moderate levels ($\sigma \approx 2$), there is a more significant increase at low frequencies ($f < 300$ Hz). On the other hand, moderate blowing rates are associated with a stronger noise attenuation of up to 15 dB at high frequencies ($f > 300$ Hz). This flow control technique has then a maximum reduction at $\sigma \approx 1.8$, beyond which increasing the blowing rate does not produce any additional benefits. Therefore, from our analysis, the largest noise reduction obtained with a perpendicular blowing is at a blowing rate of $\sigma = 1.8$, and it is achieved at frequencies of $f > 300$ Hz. The results for the blowing angle of $\alpha = 70°$ show similar trends to those of the perpendicular injection, see Fig. 4(a) and (b).

As the flow injection angle reduces to $\alpha = 50°$, the far field noise shows a very different behaviour, which can be observed in Fig. 4(c). This time, the strongest reduction in the spectral content S_{pp} is observed at the lowest blowing rate, i.e. at $\sigma = 1.3$, and the aeroacoustic benefits are progressively lost for growing blowing rates. Analogous to higher blowing angles, the noise reduction occurs at frequencies above $f = 300$ Hz. Figure 4(d) shows the estimates of the far field trailing edge noise for a blowing angle of $\alpha = 30°$. Here, noise reduction is achieved for frequencies $f > 800$ Hz, therefore over a shorter frequency range than previously found, while a noise increase is expected at frequencies lower than $f \approx 800$ Hz. Similar to the observations for the injection angle of $\alpha = 50°$, the use of the lowest blowing rate gives the largest noise attenuation.

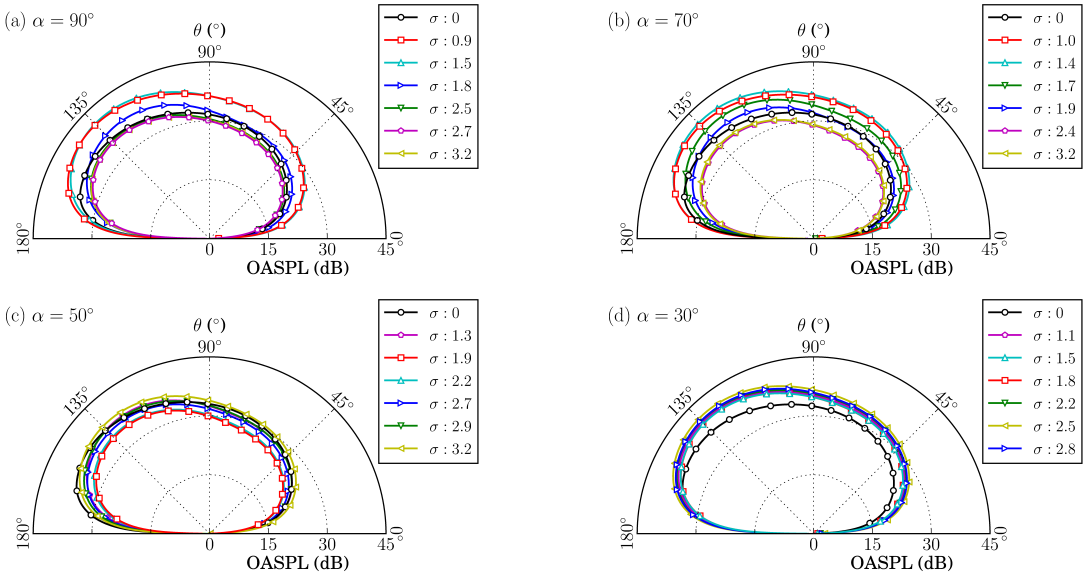

FIG. 5. Estimation of far field noise overall sound pressure level for flow injection angles of (a) $\alpha = 90°$, (b) $\alpha = 70°$, (c) $\alpha = 50°$ and (d) $\alpha = 30°$ using Amiet's trailing edge noise model with the observer located at different polar angles with a radial distance of 1 m above the trailing edge.

In order to understand the effects of flow injection on the overall far field noise, the power spectrum of the far field noise $S_{pp}(x,y,z=0,f)$ is integrated over a wide range of frequencies at varying polar angles. Specifically, an estimate for the far field noise overall sound pressure level (OASPL) is obtained at different polar angles by integrating S_{pp} between 100 Hz and 10 kHz. In Fig. 5, the OASPL is presented at four different blowing angles, i.e. at $\alpha = 90^\circ$, 70°, 50°, and 30°. In general, the behavior of the OASPL reflects that of the S_{pp} reported previously (see Fig. 4). At high injection angles ($\alpha = 90^\circ$ and 70°), the results reveal that only the use of high blowing rates ($\sigma > 2$) can reduce the overall sound pressure level. In addition, an injection angle of 70° shows better performances at high blowing rates ($\sigma > 2.0$), i.e. a stronger reduction of the OASPL, compared to the perpendicular blowing ($\alpha = 90^\circ$). This observation suggests that introducing a streamwise component to the blown-in air can favourably affect the aeroacoustic performance of the flow control system. At 50°, the results reveal that the highest reduction of the OASPL can only be achieved for low blowing rates, i.e. $\sigma \approx 2$. Finally, blowing at the most shallow flow injection angle, i.e. at $\alpha = 30^\circ$, does not lead to any reduction in OASPL, regardless of the flow control severity (see Fig. 5(d)) due to the low frequency noise increase and a higher crossing frequency (at around $f \approx$800 Hz), as previously observed in Fig. 4.

Recently, Szőke *et al.*[40] investigated the effects of flow suction on turbulent boundary layer trailing edge noise. Therefore, it would be of interest to compare the aeroacoustic performances of both uniform blowing and uniform suction, and to relate these performances to their required power consumption. From Fig. 5, the largest trailing edge noise reduction in OASPL for an observer located above the trailing edge is found to be 3 dB, which is obtained at a blowing rate of $\sigma \approx 2$. This is equivalent to injecting air flow corresponding to 20% of the boundary layer thickness[52]. However, applying flow suction at a rate of $\sigma \approx 2$ (i.e. removing 20% of the boundary layer thickness) was found to reduce the OASPL only by 2 dB for the same observer location[40]. Therefore, at lower flow control severity ($\sigma \approx 2$) inclined flow injection offers a better aeroacoustic performance than flow suction. However, flow suction has significantly higher noise reduction potentials than blowing provided that the limitations on the energy requirements can be relaxed. For instance, it was found[40] that removing 60% of the boundary layer thickness ($\sigma \approx 6$) provides 6 dB attenuation of the estimated trailing edge noise. Therefore, at higher flow control severity rates flow suction offers a better aeroacoustic performance then flow injection.

IV. THE FLOW FIELD

The previous section revealed how blowing affects the trailing edge noise. The acoustic effects of blowing was examined through the two quantities whose product drives the generation of trailing edge noise, namely, the power spectral density of the surface pressure fluctuations and the spatial extent of the turbulent structures. In this section, we analyze the velocity data from hot-wire anemometry to gain a better understanding of the flow field downstream of the flow control area, in proximity to the trailing edge. This analysis has two main objectives, (i) to provide a physical explanation for the observed aeroacoustic performances of uniform blowing, (ii) to qualitatively evaluate how this technique of noise attenuation may affect the aerodynamics of the flow over the flat plate.

A. Mean and root mean square velocity profiles

Mean and root mean square (r.m.s.) velocity profiles are obtained from measurements of hot-wire anemometry at the four downstream locations (BL1, BL2, BL3 and BL4), and they are shown in Fig. 6. The distance of these measurement stations from the flow control area is reported in Table I, nondimensionalised by the thickness of the undisturbed boundary layer, δ_0. Note that we chose to present these velocity profiles only for injection angles of $\alpha = 90^\circ$ (Fig. 6, top) and of $\alpha = 50^\circ$ (Fig. 6, bottom). This is because the estimates of the trailing edge noise reported in Section III C show that uniform blowing at $\alpha = 90^\circ$ and at $\alpha = 70^\circ$ produces similar aeroacoustic performances, whereas uniform blowing at $\alpha = 30^\circ$ leads to an increase of trailing edge noise emissions, which makes it a case of scarce interest.

An inspection of the mean velocity profiles downstream of the uniform blowing at $\alpha = 90^\circ$ (see Fig. 6(a)) shows that the boundary layer velocity profiles are very sensitive to the blowing rate (σ). At low blowing rates, i.e. $\sigma = 0.9$ (red squares), flow injection produces a modest effect on the mean velocity profiles, which do not deviate significantly from the base velocity profiles (black circles). When doubling the blowing rate ($\sigma = 1.8$, blue triangles), the footprint of a separation bubble on the velocity profile can be observed, with a reattachment of the flow occurring between BL2 and BL3. At a uniform blowing of $\sigma = 2.7$, at the highest blowing rate tested here, the flow clearly exhibits a separation that persists until the trailing edge. Although for a uniform blowing at $\alpha = 90^\circ$ the mean velocity profiles are very sensitive to the blowing rate, a modest sensitivity is

observed when blowing at $\alpha = 50°$ (bottom left). For a uniform blowing of $\alpha = 50°$ (see Fig. 6(c)), the profiles of mean velocity resemble the one obtained for a blowing rate of $\sigma = 1.8$ at $\alpha = 90°$. The footprint of a separation bubble is observed at BL2, followed by a reattachment of the flow.

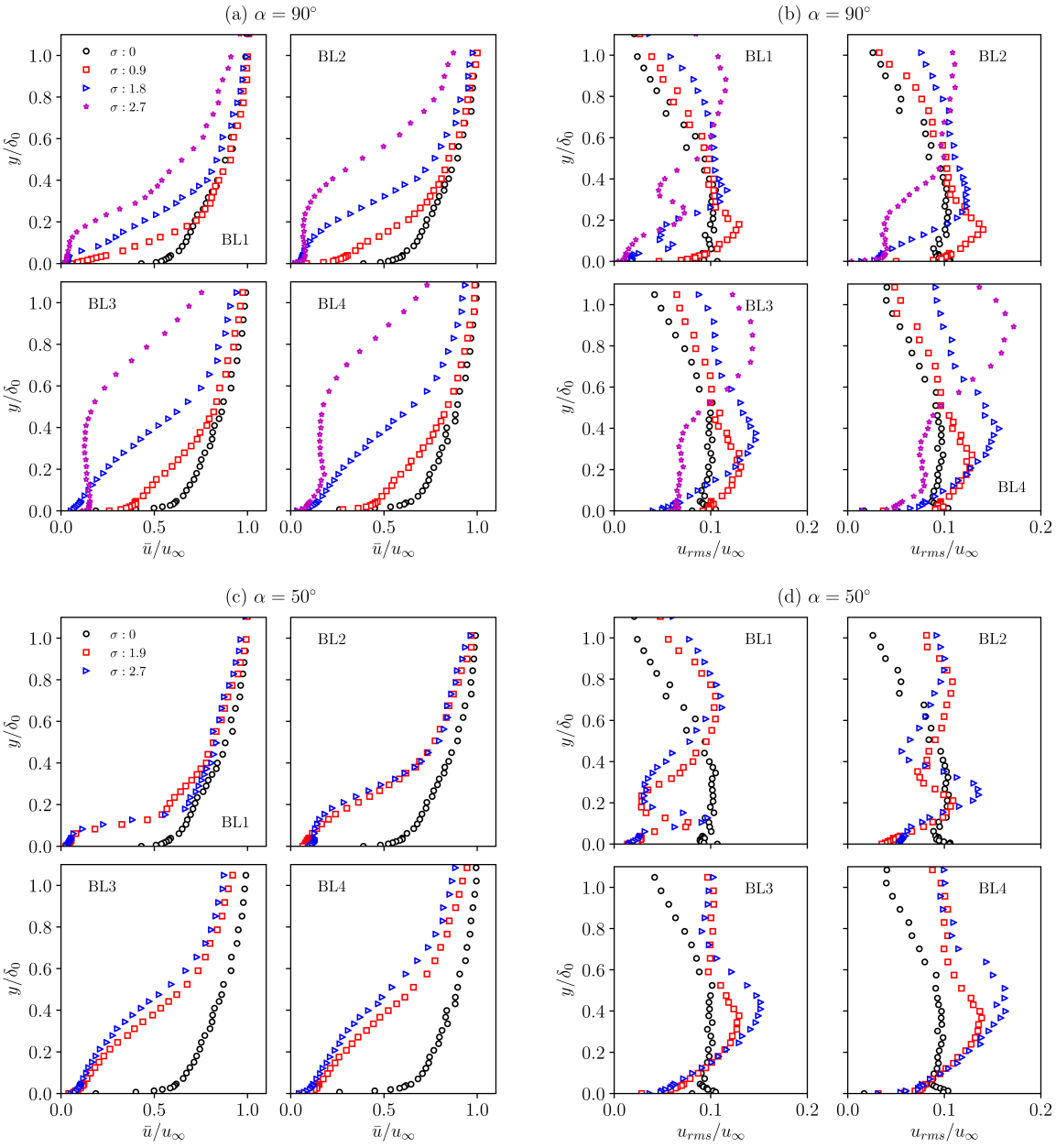

FIG. 6. (a,c) Mean and (b,d) root mean square velocity profiles measured at a flow injection angles of $\alpha = 90°$ (a,b) and $\alpha = 50°$ (c,d), at locations BL1-BL4.

Up to here, the profiles of mean velocity have been discussed. In order to know more about how the flow structure is affected by uniform blowing, the r.m.s velocity profiles are presented in the

right column of Fig. 6. The r.m.s. of the velocity represents the turbulent kinetic energy within the boundary layer. When blowing at an angle of $\alpha = 90°$, a prominent maximum can be observed in each of the three r.m.s. profiles obtained from the three blowing rates, see Fig. 6(b). Considering all streamwise locations under analysis (BL1-BL4), the maximum of each r.m.s. velocity profile moves toward higher wall-normal locations and the r.m.s. content becomes larger for increasing blowing rates. At the same wall-normal distance (y/δ_0) where the peaks are observed in the r.m.s. profiles, the mean velocity results have an inflection point. This is very well visible for $\sigma = 2.7$ at $\alpha = 90°$, see Fig. 6(a,b). Below the inflection point, the magnitude of the mean velocity is significantly lower than the free-stream velocity. The simultaneous presence of a prominent peak in the r.m.s. profiles and an inflection point in the mean velocity results confirm that a shear layer is embedded into the boundary layer[55,56]. A separation bubble is present below the inflection point, and the core of the shear layer is located at the inflection point. Another observation is that when blowing at $\sigma = 2.7$, the energy content in the range of wall-normal locations $y/\delta_0 < 0.5$ is much lower than that of the base turbulent boundary layer, regardless of the location downstream of the flow control area. Assuming a proportionality between the boundary layer energy content and the surface pressure fluctuations, this observation could explain the noise attenuation observed in the previous section. Finally, we examine the r.m.s. profiles downstream of a flow injection at $\alpha = 50°$, see Fig 6(d). After a short transitory, the shear layer at the top edge of the separation bubble seems to be fully-developed by BL3. The effect of blowing induces the formation of a maximum in each r.m.s. velocity profile, regardless of the blowing angle (α) or flow control severity (σ). This is a similar observation to what was found at an injection angle of $\alpha = 90°$. Analogous to that, higher blowing rates shift the maximum r.m.s. toward larger wall-normal locations, and strengthen the maximum itself. However, when blowing at $\alpha = 50°$, the location of the peak in the r.m.s. profiles, i.e. the core of the shear layer, remains closer to the wall at all investigated streamwise locations (BL1-BL4).

From the analysis of the mean and r.m.s. velocity profiles, the flow developing downstream of the flow control section can be classified in three possible scenarios, depending on the angle of injection and the blowing rate. These scenarios correspond to the different flow patterns presented in Fig. 7. The first flow pattern is shown in Fig. 7(a), and it is typical of low blowing rates ($\sigma \approx 1$) independent of the injection angle, and of $\alpha = 30°$ regardless of the blowing rate, although the velocity profiles associated to these latter cases are not reported here. In this flow pattern, no flow separation occurs, even if an incipient separation extending over a very short downstream distance

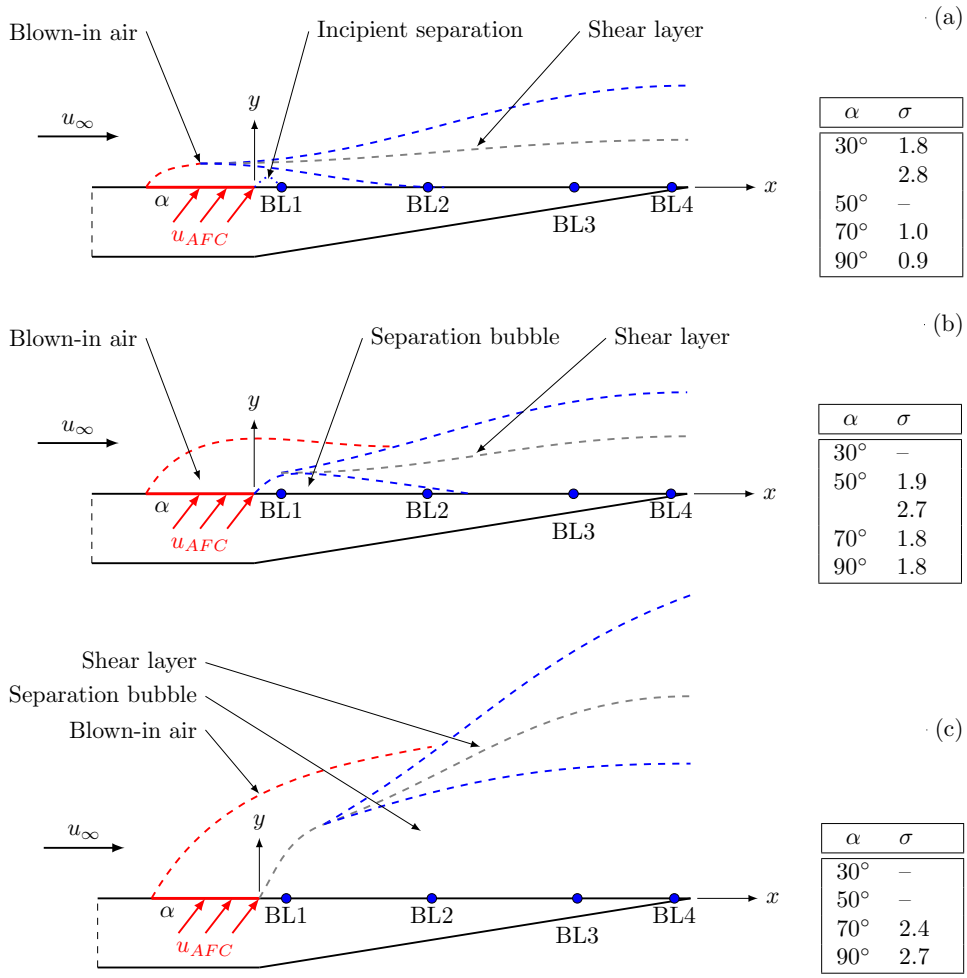

α	σ
30°	1.8
	2.8
50°	–
70°	1.0
90°	0.9

α	σ
30°	–
50°	1.9
	2.7
70°	1.8
90°	1.8

α	σ
30°	–
50°	–
70°	2.4
90°	2.7

FIG. 7. Conceptual schematics illustrating the flow patterns in three possible scenarios of active flow control through uniform blowing: (a) low blowing rates, (b) medium blowing rates and (c) high blowing rates. The conditions of flow control leading to the related flow patterns are presented in the tables on the right.

between the end of the flow control area and BL1 cannot be excluded from the available data. The injected air creates a sort of barrier, which tends to decelerate the incoming flow near the wall, leading to the formation of a shear layer at wall-normal locations $y/\delta_0 < 0.4$. The wall-normal position of the shear layer roughly corresponds to the maximum of the r.m.s. velocity profile, as previously seen in Fig. 6. The second flow pattern is shown in Fig. 7(b), and it is typical of all the examined blowing rates at an injection angle of $\alpha = 50°$, and of a medium blowing rate ($\sigma \approx 1.5-2$) at injection angles of $\alpha = 70°$ and $\alpha = 90°$. A separation bubble appears immediately downstream of flow injection, whose footprint can be observed from the profiles of mean velocity at BL1 and BL2. As can be observed from the peak in the r.m.s. and inflection point in the mean

velocity profiles in Fig. 6, downstream of BL2 the flow reattaches, therefore no flow separation is present at BL3 and BL4. A shear layer is embedded in the boundary layer, although its wall-normal position is higher than in the flow pattern previously described, i.e. at $y/\delta_0 \approx 0.5$. Again, the locations of the r.m.s. velocity peak enable us to identify the wall-normal position of the shear layer, as seen in Fig. 6. The third flow pattern is shown in Fig. 7(c). The flow downstream of the flow control area is fully separated as a result of high blowing rates ($\sigma > 2$) at injection angles of $\alpha = 70^\circ$ and $\alpha = 90^\circ$. Based on the far field noise results presented in Fig. 4, high blowing rates and high injection angles cause a significant reduction in the far field noise. However, this noise reduction can now be explained as a consequence of flow separation upstream or over the trailing edge.

Our observations regarding the mean and r.m.s. velocity profiles and the flow patterns downstream of the flow control area are in good agreement with the findings of Park and Choi[44] and Kametani and Fukagata[45], who performed numerical simulations on the problem of perpendicular flow injection into a turbulent boundary layer. They also found that perpendicular blowing lifts the streamwise vortices away from the wall, and it increases the turbulence intensity downstream of the flow control area. As discussed in Section I, understanding the changes to the boundary layer structure is at the basis of interpreting how flow injection can reduce trailing edge noise. The following paragraphs aim to find links between the spectral content of the surface pressure fluctuations and the spectral content of the velocity fluctuations within the boundary layer. This can help us to identify which areas of the flow are responsible for increasing or decreasing the trailing edge noise.

B. Velocity power spectral density

The analysis of the r.m.s. velocity profiles revealed that uniform blowing can significantly change the energy content of the boundary layer downstream of the flow control area. Based on our observations from Fig. 6(b,d), flow injection increases the turbulence levels at locations away from the wall, while in the near-wall region, the turbulent kinetic energy decreases. Despite the useful information obtained from the r.m.s. velocity data (see Fig. 6), the frequency-energy content of the boundary layer structures are not yet known. These aspects can be clarified from investigating the velocity power spectral density (ϕ_{uu}, dB/Hz) at different flow control parameters. Figure 8 presents the difference between the power spectral density of the velocity fluctuations in the presence of

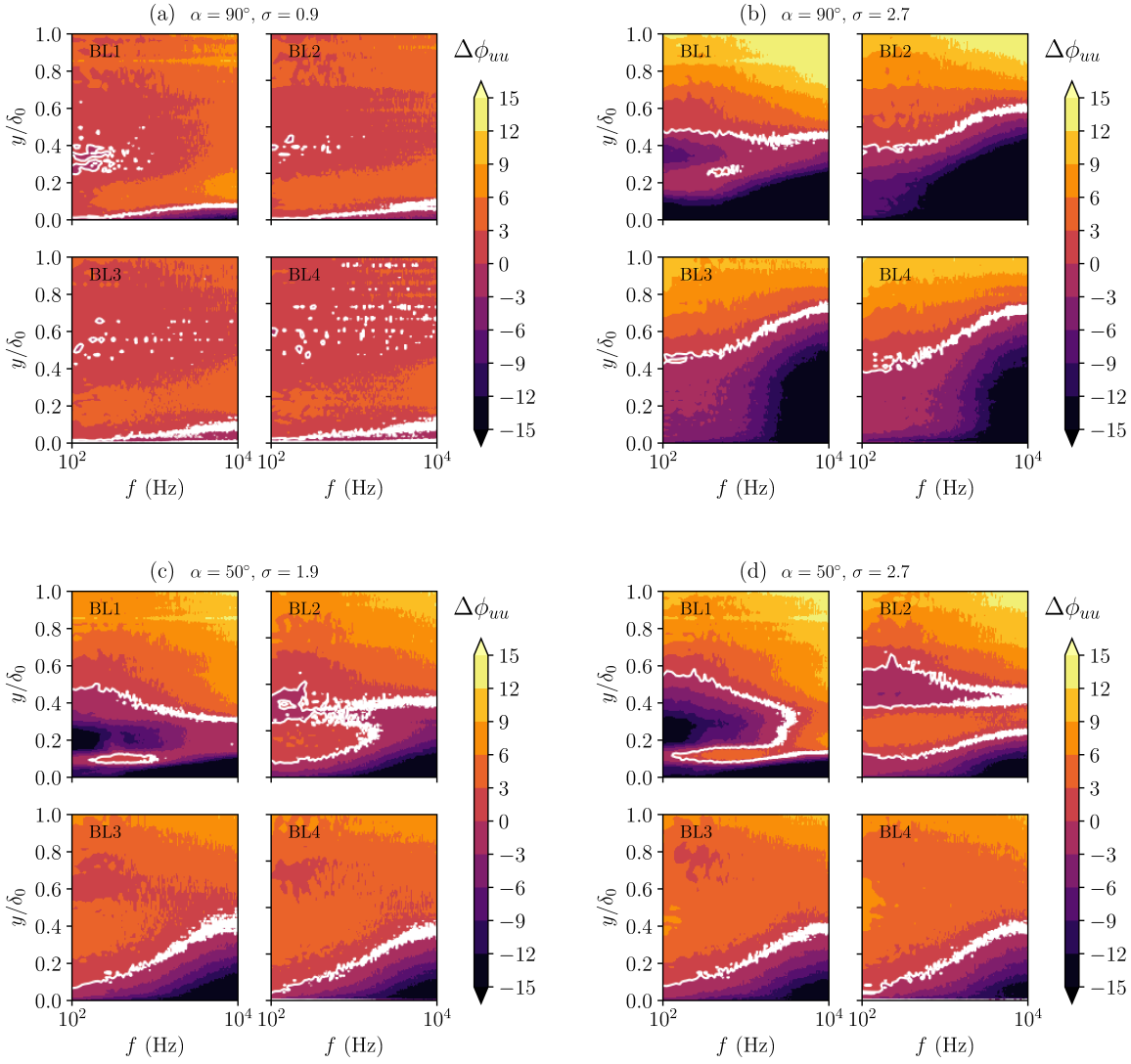

FIG. 8. Changes in the velocity power spectral density ($\Delta\phi_{uu}$) for flow injection angle of $\alpha = 90°$ (a,b) and of $\alpha = 50°$ (c,d) at different blowing rates, at locations BL1-BL4. The white areas correspond to $\Delta\phi_{uu} = 0$ dB/Hz.

flow injection ($\phi_{uu,\sigma\neq 0}$), and the power spectral density of the velocity fluctuations of the baseline case ($\phi_{uu,\sigma=0}$), i.e. $\Delta\phi_{uu} = \phi_{uu,\sigma\neq 0} - \phi_{uu,\sigma=0}$, for different blowing rates and injection angles. Positive changes denote an increase in the spectral content with respect to the base boundary layer, while negative changes are associated with a reduction in the flow energy content. The iso-levels of no change, i.e. $\Delta\phi_{uu} = 0$, in the velocity power spectral density are marked with white contour lines. At a first glimpse, uniform blowing produces a broadband increase of the velocity spectral content in the outer region of the turbulent boundary layer while it leads to a reduction in

the near-wall region. This is a general effect, resulting from uniform blowing, and it appears for all the examined injection angles and blowing rates.

In Fig. 8(a), the effects of blowing at an angle of $\alpha = 90^\circ$ and at a blowing rate of $\sigma = 0.9$ are shown. As can be seen, uniform blowing reduces the energy content at BL1, i.e. close to the flow control unit, particularly at high frequencies ($f > 1$ kHz). However, when moving farther downstream, this effect weakens significantly, and by BL4 only a modest energy reduction is experienced below $y/\delta_0 = 0.1$. These observations are consistent with the mild noise reduction found at high frequencies in ϕ_{pp} and S_{pp}, see Fig. 2 and 4. In Fig. 8(b), the effects of a larger blowing rate of $\sigma = 2.7$ at an angle of $\alpha = 90^\circ$ are examined. The flow control produces a broadband reduction of the energy content near the wall ($y/\delta_0 < 0.5$), and this reduction is much stronger at high frequencies ($f > 1$ kHz). At low frequencies ($f < 1$ kHz), the reduction of the velocity spectrum is strong at BL1, and it gradually decreases toward the trailing edge. However, the energy reduction at high frequencies appears to be similar in structure over all locations under analysis (BL1-BL4). The spectra of the surface pressure fluctuations (see Fig. 2) reflect the observed trend, with implications on the estimated trailing edge noise.

Changes in the power spectral density for an injection angle of $\alpha = 50^\circ$ are presented in Fig. 8(c,d). As can be seen, a blowing rate of $\sigma = 1.9$ causes a strong reduction of the velocity power spectral density at high frequencies ($f >$400 Hz), which is most significant at locations BL3 and BL4. The reduction gained at low frequencies ($f <$400 Hz), however, is almost completely lost by BL3 and BL4, and we can observe an increase in the flow energy content for wall-normal locations $y/\delta_0 > 0.1$. This scenario is consistent with the spectra of the surface pressure fluctuations and with the r.m.s. velocity profiles. Increasing the blowing rate up until $\sigma = 2.7$ does not produce significant changes, as can be observed when comparing Fig. 8(c) and Fig. 8(d). However, at $y/\delta_0 > 0.2$, therefore conveniently far from the wall, a larger increase in the energy content can be observed when blowing at $\sigma = 2.7$, especially at low frequencies ($f < 400$ Hz). This is again consistent with the r.m.s. velocity profiles, and explains why the spectral density of the surface pressure fluctuations is larger when blowing at $\sigma = 2.7$ than when blowing at $\sigma = 1.9$, as observed in Fig. 2.

In conclusion, flow injection can reduce the energy content within the turbulent boundary layer by introducing a layer of air in the near-wall region characterised by low turbulence intensity, and at the same time, by shifting the turbulent structures of the boundary layer away from the wall. In combination, these two mechanisms are observed to reduce the trailing edge noise at mid and high

frequencies. On the other hand, flow injection leads to the formation of a region of low-momentum near the wall, and the interaction between this low-momentum region and the turbulent boundary layer produces a shear layer. The core of the shear layer is located at higher wall-normal positions as the blowing rate increases. This shear layer "steals" energy from the mean flow and "turns" it into turbulent kinetic energy at large turbulence scales. From a hydrodynamic point of view, this larger energy content away from the wall generates, as a footprint, a stronger spectral content of the surface pressure fluctuations, which is ultimately responsible for an increase of the trailing edge noise at low frequencies.

V. CONCLUSIONS

The hydrodynamic effects of uniform injection on a zero pressure gradient turbulent boundary layer developing over a flat plate were investigated experimentally. The effects of two flow control parameters were examined, namely, the angle of injection (α) and the blowing rate (σ). Four injection angles, defined as the angle between the injected air and the free-stream velocity, were considered, namely, $\alpha = 30^\circ, 50^\circ, 70^\circ, 90^\circ$. The blowing rate relates the momentum of the injected air to the momentum deficit of the turbulent boundary layer, and this parameter was varied in the experiments between $\sigma = 0$ and 3.2. Uniform blowing was applied in an open-loop manner of control, upstream of the flat plate trailing edge.

In the first part of the study, the far field trailing edge noise was calculated through Amiet's model[9], using signals of surface pressure fluctuations from flush-mounted microphones. Noise reduction of up to 15 dB was found at mid and high frequencies ($f > 300$ Hz) when applying a blowing rate of $\sigma \gtrsim 2$ at injection angles of $\alpha = 70^\circ$ and $\alpha = 90^\circ$. However, this noise reduction was always accompanied by an increase of trailing edge noise at low frequencies. Analogous performances were found for flow injection of $\sigma \approx 1.5 - 2$ and at an angle of $\alpha = 50^\circ$. The spectrum of the estimated trailing edge noise appeared similar to that of the surface pressure fluctuations in the close proximity of the trailing edge, which highlights the dominance of this term in Amiet's model. The analysis of the overall sound pressure level revealed a noise reduction for the strongest values of σ that were tested ($\sigma > 2.5$), and for injection angles of $\alpha = 70^\circ$ and $\alpha = 90^\circ$. For an injection angle of $\alpha = 50^\circ$, a similar noise reduction was obtained, although for significantly lower blowing rates, i.e. $\sigma \approx 1.5 - 2$. Uniform blowing at an angle of $\alpha = 30^\circ$ generally leads to an increase of the trailing edge noise and was therefore considered a configuration of scarce interest.

In the second part of the study, we examined the flow field downstream of the flow control treatment through velocity signals from hot-wire anemometry. The mean velocity profiles revealed that strong uniform blowing ($\sigma > 2$) at high angles ($\alpha = 70^\circ$ and 90°) produces a flow separation. On the other hand, flow injection at $\alpha = 50^\circ$ and at a blowing rate of $\sigma \approx 1.5 - 2$ leads to the formation of a separation bubble immediately downstream of the flow control area, which is followed by flow reattachment. This makes uniform blowing at $\alpha = 50^\circ$ and at a blowing rate of $\sigma \approx 1.5 - 2$ the most promising configuration from the currently investigated cases because this configuration offers aeroacoustic performances similar to those obtained at higher angles and at strong blowing rates, but it does not lead to flow separation, and it requires less external power input. Finally, the analysis of the r.m.s. velocity profiles showed that, for all the examined cases, uniform blowing produces a shear layer whose wall-normal position increases with the injection angle and with the blowing rate. The formation of this shear layer was linked with the generation of far field noise at low frequencies. Direct measurements of far field trailing edge noise in an anechoic wind tunnel accompanied with lift and drag tests should be performed to confirm the observations presented in this paper.

DATA AVAILABILITY

The data that support the findings of this study are available from the corresponding author upon reasonable request.

REFERENCES

[1]T. F. Brooks and T. H. Hodgson, "Trailing edge noise prediction from measured surface pressures," Journal of Sound and Vibration **78(1)**, 69–117 (1981).

[2]T. F. Brooks, D. S. Pope, and M. A. Marcolini, "Airfoil self-noise and prediction," NASA Report **1218** (1989).

[3]B. Arnold, T. Lutz, E. Krämer, and C. Rautmann, "Wind-turbine trailing-edge noise reduction by means of boundary-layer suction," AIAA Journal **56(5)**, 1843–1854 (2018).

[4]A. Wolf, T. Lutz, W. Würz, E. Krämer, O. Stalnov, and A. Seifert, "Trailing edge noise reduction of wind turbine blades by active flow control," Wind Energy **1737** (2014).

[5]J. E. Ffowcs-Williams and D. L. Hawkings, "Sound generation by turbulence and surfaces in arbitrary motion," Philosopical Transactions of the Royal Society London **264**, 321–342 (1969).

[6]J. E. Ffowcs-Williams and L. H. Hall, "Aerodynamic sound generation by turbulent flow and in the vicinity of a scattering half plane," Journal of Fluid Mechanics **40(4)**, 657–670 (1970).

[7]R. Amiet, "Acoustic radiation from an airfoil in a turbulent stream," Journal of Sound and Vibration **41**, 407–420 (1975).

[8]D. M. Chase, "Noise radiated from an edge in turbulent flow," AIAA Journal **13**, 1041–1047 (1975).

[9]R. Amiet, "Noise due to turbulent flow past a trailing edge," Journal of Sound and Vibration **47(3)**, 387–393 (1976).

[10]B. Lyu, M. Azarpeyvand, and S. Sinayoko, "Prediction of noise from serrated trailing edges," Journal of Fluid Mechanics **793**, 556–588 (2016).

[11]M. Gruber, *Airfoil noise reduction by edge treatments*, Ph.D. thesis, University of Southampton, UK. (2012).

[12]X. Liu, H. J. Kamliya, M. Azarpeyvand, and R. Theunissen, "Wake Development of Airfoils with Serrated Trailing Edges," 22nd AIAA/CEAS Aeroacoustics Conference (AIAA-2016-2817).

[13]F. Avallone, S. Pröbsting, and D. Ragni, "Three-dimensional flow field over a trailing-edge serration and implications on broadband noise," Physics of Fluids **28**, 117101 (2016).

[14]M. Gruber, P. Joseph, and M. Azarpeyvand, "An experimental investigation of novel trailing edge geometries on airfoil trailing edge noise reduction," 19th AIAA/CEAS Aeroacoustics Conference (AIAA-2013-2011).

[15]M. Azarpeyvand, M. Gruber, and P. Joseph, "An analytical investigation of trailing edge noise reduction using novel serrations," 19th AIAA/CEAS Aeroacoustics Conference (AIAA-2013-2009).

[16]S. L. Prigent, O. R. H. Buxton, and P. J. K. Bruce, "Coherent structures shed by multiscale cut-in trailing edge serrations on lifting wings," Physics of Fluids **29**, 075107 (2017).

[17]A. Finez, E. Jondeau, M. Roger, and M. Jacob, "Broadband noise reduction with trailing edge brushes," in *16th AIAA/CEAS Aeroacoustics Conference, Stockholm, Sweden* (AIAA-2010-3980).

[18]M. Herr and W. Dobrzynski, "Experimental investigations in low-noise trailing-edge design," AIAA Journal **43(6)**, 1167–1175 (2005).

[19]T. Geyer, E. Sarradj, and C. Fritzsche, "Measurement of the noise generation at the trailing edge of porous airfoils," Experiments in Fluids **48**, 291–308 (2010).

[20]Y. Bae and Y. J. Moon, "Effect of passive porous surface on the trailing-edge noise," Physics of Fluids **23**, 126101 (2011).

[21]S. A. Showkat Ali, M. Azarpeyvand, and C. R. Ilário da Silva, "Trailing-edge flow and noise control using porous treatments," Journal of Fluid Mechanics **850**, 83–119 (2018).

[22]S. Showkat Ali, X. Liu, and M. Azarpeyvand, "Bluff body flow and noise control using porous media," 22nd AIAA/CEAS Aeroacoustics Conference, Lyon, France (AIAA-2016-2754).

[23]S. A. Showkat Ali, M. Szőke, and M. Azarpeyvand, "Trailing edge bluntness flow and noise control using porous treatments," 22nd AIAA/CEAS Aeroacoustics Conference, Lyon, France (AIAA-2016-2832).

[24]S. A. Showkat Ali, M. Azarpeyvand, M. Szőke, and C. R. Ilário da Silva, "Boundary layer flow interaction with a permeable wall," Physics of Fluids **30**, 085111 (2018).

[25]H. Liu, M. Azarpeyvand, J. Weia, and Z. Qua, "Tandem cylinder aerodynamic sound control using porous coating," Journal of Sound and Vibration , 190–201 (2014).

[26]A. Rubio Carpio, F. Avallone, D. Ragni, M. Snellen, and S. van der Zwaag, "Mechanisms of broadband noise generation on metal foam edges," Physics of Fluids **31**, 105110 (2019).

[27]S. A. S. Ali, M. Azarpeyvand, and C. R. I. da Silva, "Trailing edge bluntness noise reduction using porous treatments," Journal of Sound and Vibration **474**, 115257 (2020).

[28]A. Afshari, M. Azarpeyvand, A. A. Dehghan, and M. Szőke, "Trailing edge noise reduction using novel surface treatments," *22nd AIAA/CEAS Aeroacoustics Conference*, 22nd AIAA/CEAS Aeroacoustics Conference, Lyon, France (AIAA-2016-2834).

[29]A. Afshari, M. Azarpeyvand, A. A. Dehghan, and M. Szőke, "Three-dimensional surface treatments for trailing edge noise reduction," 23rd International Congress on Sound & Vibration, Athens, Greece (2016).

[30]I. Clark, D. Baker, W. N. Alexander, W. Devenport, S. A. Glegg, J. Jaworski, and N. Peake, "Experimental and theoretical analysis of bio-inspired trailing edge noise control devices," in *22nd AIAA/CEAS Aeroacoustics Conference* (AIAA-2016-3020).

[31]I. Clark, W. N. Alexander, W. Devenport, S. A. Glegg, J. Jaworski, C. Daily, and N. Peake, "Bio-inspired trailing edge noise control," in *21st AIAA/CEAS Aeroacoustics Conference* (AIAA-2015-2365).

[32]A. Afshari, M. Azarpeyvand, A. A. Dehghan, M. Szőke, and R. Maryami, "Trailing-edge flow manipulation using streamwise finlets," Journal of Fluid Mechanics **870**, 617–650 (2019).

[33]A. Gonzalez, S. A. Glegg, N. Hari, and W. J. Devenport, "Fundamental studies of the mechanisms of pressure shielding," in *25th AIAA/CEAS Aeroacoustics Conference* (AIAA-2019-2403).

[34]Q. Ai, M. Azarpeyvand, X. Lachenal, and P. M. Weaver, "Aerodynamic and aeroacoustic performance of airfoils with morphing structures," Wind Energy **19**, 1325–1339 (2016).

[35]H. Kamliya Jawahar, Q. Ai, and M. Azarpeyvand, "Aerodynamic and aeroacoustic performance of airfoils fitted with morphing trailing-edges," in *2018 AIAA/CEAS Aeroacoustics Conference* (AIAA-2018-2815).

[36]P. M. Hartwich, E. D. Dickey, A. J. Sclafani, P. Camacho, A. B. Gonzales, E. L. Lawson, R. Y. Mairs, and A. Shmilovich, "Afc-enabled simplified high-lift system integration study," (2014).

[37]M. Koklu, "Effect of a coanda extension on the performance of a sweeping-jet actuator," AIAA Journal **54**, 1131–1134 (2016).

[38]D. Matera, *Validation of the noise prediction code Rnoise and reduction of trailing edge noise by active flow control*, Ph.D. thesis, Universita Degli Studi Di Padova (2013).

[39]T. Lutz, B. Arnold, A. Wolf, and E. Krämer, "Numerical studies on a rotor with distributed suction for noise reduction," Journal of Physics: Conference Series **524**, 012122 (2014).

[40]M. Szőke, D. Fiscaletti, and M. Azarpeyvand, "Influence of boundary layer flow suction on trailing edge noise generation," Journal of Sound and Vibration **475**, 115276 (2020).

[41]S. Moreau, P. Laffay, A. Idier, and N. Atalla, "Several noise controls of the trailing-edge noise of a controlled-diffusion airfoil," in *22nd AIAA/CEAS Aeroacoustics Conference, Lyon, France* (AIAA-2016-2816).

[42]M. Szőke, D. Fiscaletti, and M. Azarpeyvand, "Effect of inclined transverse jets on trailing-edge noise generation," Physics of Fluids **30**, 085110 (2018).

[43]R. Antonia, Y. Zhu, and M. Sokolov, "Effect of concentrated wall suction on a turbulent boundary layer," Physics of Fluids **7**, 2465–2474 (1995).

[44]J. Park and H. Choi, "Effects of uniform blowing or suction from a spanwise slot on a turbulent boundary layer flow," Physics of Fluids **11**, 3095 (1999).

[45]Y. Kametani and K. Fukagata, "Direct numerical simulation of spatially developing turbulent boundary layers with uniform blowing or suction," Journal of Fluid Mechanics **681**, 154–172 (2011).

[46]A. Silvestri, F. Ghanadi, M. Arjomandi, R. Chin, B. Cazzolato, and A. Zander, "Attenuation of turbulence by the passive control of sweep events in a turbulent boundary layer using micro-cavities," Physics of Fluids **29**, 115102 (2017).

[47]S. Qin, N. Chu, Y. Yao, J. Liu, B. Huang, and D. Wu, "Stream-wise distribution of skin-friction drag reduction on a flat plate with bubble injection," Physics of Fluids **29**, 037103 (2017).

[48]S. Tamano, H. Uchikawa, J. Ito, and Y. Morinishi, "Streamwise variations of turbulence statistics up to maximum drag reduction state in turbulent boundary layer flow due to surfactant injection," Physics of Fluids **30**, 075103 (2018).

[49]H. Lee, B. Wen, and C. R. Doering, "Improved upper bounds on the energy dissipation rate for shear flow with injection and suction," Physics of Fluids **31**, 085102 (2019).

[50]M. Szőke and M. Azarpeyvand, "Active flow control methods for the reduction of trailing edge noise," in *23rd AIAA/CEAS Aeroacoustics Conference* (AIAA-2017-3004).

[51]M. Szőke, *Trailing Edge Noise Control Using Active Flow Control Methods*, Ph.D. thesis, University of Bristol (2019).

[52]R. Antonia, Y. Zhu, and M. Sokolov, "Effect of concentrated wall suction on a turbulent boundary layer," Physics of Fluids **7**, 2465–2474 (1995).

[53]R. R. Parchen and Technisch Physisce Dienst, "Progress report DRAW: A prediction scheme for trailing edge noise based on detailed boundary layer characteristics," TNO Report **(HAG-RPT-980023)** (1998).

[54]M. Roger and S. Moreau, "Broadband self-noise from loaded fan blades," AIAA Journal **42(3)**, 536–544 (2004).

[55]D. M. Schatzman and F. O. Thomas, "An experimental investigation of an unsteady adverse pressure gradient turbulent boundary layer: embedded shear layer scaling," Journal of Fluid Mechanics **815**, 592–642 (2017).

[56]N. A. Balantrapu, D. J. Fritsch, A. J. Millican, C. Hickling, A. Gargiulo, V. Vishwanathan, W. N. Alexander, and W. J. Devenport, "Wall pressure fluctuations in an axisymmetric turbulent boundary layer under strong adverse pressure gradient," in *AIAA Scitech 2020 Forum* (AIAA-2020-0572).